Published in final edited form as:
Neurogenetics. 2011 August ; 12(3): 223–232. doi:10.1007/s10048-011-0285-6.

A novel *mitofusin 2* mutation causes canine fetal-onset neuroaxonal dystrophy

John C. Fyfe, DVM, PhD[1], **Raba' A. Al-Tamimi, PhD**[1], **Junlong Liu, MD**[2], **Alejandro A. Schäffer, PhD**[3], **Richa Agarwala, PhD**[3], and **Paula S. Henthorn, PhD**[2]

[1]Laboratory of Comparative Medical Genetics, Department of Microbiology & Molecular Genetics, College of Veterinary Medicine, Michigan State University, East Lansing, MI 48824

[2]Section of Medical Genetics, School of Veterinary Medicine, University of Pennsylvania, Philadelphia, PA 19104

[3]National Center for Biotechnology Information, National Institutes of Health, Department of Health and Human Services, Bethesda, MD 20894

Abstract

We recently reported autosomal recessive fetal-onset neuroaxonal dystrophy (FNAD) in a large family of dogs that is not caused by mutation in the *PLA2G6* locus (2010 J Comp Neurol 518:3771–3784). Here we report a genome-wide linkage analysis using 333 microsatellite markers to map canine FNAD to the telomeric end of chromosome 2. The interval of zero recombination was refined by single nucleotide polymorphism (SNP) haplotype analysis to ~ 200 kb, and the included genes were sequenced. We found a homozygous 3-nucleotide deletion in exon 13 of *mitofusin 2* (*MFN2*), predicting loss of a glutamate residue at position 539 in the protein of affected dogs. RT-PCR demonstrated near normal expression of the mutant mRNA, but MFN2 expression was undetectable to very low on western blots of affected dog brainstem, cerebrum, kidney, and cultured fibroblasts and by immunohistochemistry on brainstem sections. MFN2 is a multifunctional, membrane-bound GTPase of mitochondria and endoplasmic reticulum most commonly associated with human Charcot-Marie-Tooth disease type 2A2. The canine disorder extends the range of *MFN2*-associated phenotypes and suggests *MFN2* as a candidate gene for rare cases of human FNAD.

Keywords

Neuroaxonal dystrophy; mitofusin 2; linkage analysis; animal model; disease gene

INTRODUCTION

Neuroaxonal dystrophy (NAD) is a diagnostically nonspecific, but histologically distinct neurodegenerative pathology of the central and/or peripheral nervous system characterized by local swellings (spheroids) and atrophy of axons. One of the childhood disorders in which NAD occurs as the primary pathology is recessive infantile neuroaxonal dystrophy (INAD; OMIM #256600; a.k.a. Seitelberger disease), most often caused by mutation of a gene encoding calcium-independent, group VI phospholipase A2 (*PLA2G6*) [1, 2]. Onset of signs is typically between 6 and 18 months of age and follows a progressive course of cognitive and motor regression, hypotonia, and progressive paraplegia. Patients

Corresponding author: John C. Fyfe, DVM, PhD, Laboratory of Comparative Medical Genetics, 2209 Biomedical Physical Sciences, Michigan State University, East Lansing, MI 48824 USA, Voice: 517-884-5348, FAX: 517-353-8957, fyfe@cvm.msu.edu.

characteristically exhibit cerebellar and optic atrophy and spheroids in CNS and peripheral nerve axons [3–6]. Some INAD patients also accumulate iron in the globus pallidus and/or substantia nigra. Among atypical cases of INAD are reports of disease for which the genetic etiology is unknown but that indicate onset of pathology during fetal life (so-called connatal INAD). These are a unique group in which patients exhibit early, severe motor dysfunction causing fetal akinesia and the resulting constellation of morphologic and developmental abnormalities [7–9]. In the most recent of these reports, *PLA2G6* mutation was largely excluded by sequencing the exons and splice junctions [9].

Recently we described autosomal recessive, fetal-onset neuroaxonal dystrophy (FNAD) causing late-gestational fetal akinesia, multiple joint fixation, and pulmonary hypoplasia in a large family of dogs [10] that mimics the connatal human phenotype. Affected fetuses exhibited swollen axons/spheroids throughout the extrapyramidal motor system of brainstem, spinal cord, and peripheral nerves and died at birth due to respiratory failure. They also exhibited cerebellar hypoplasia with degeneration of Purkinje cells and neurons of deep cerebellar nuclei. There was no accumulation of brain iron. The histopathologic findings and electron microscopic features of spheroids were similar to those of human INAD, but genetic markers flanking canine *PLA2G6* locus did not segregate with the disorder. Lacking functional candidate genes, we undertook and now report results of a genome-wide scan for linkage and subsequent fine-mapping of the canine FNAD locus. We demonstrate a unique mutation of *mitofusin 2* (*MFN2*) in affected dogs that abrogates MFN2 expression in brainstem and other tissues. *MFN2* is a well known disease gene in Charcot-Marie-Tooth disease type 2A (CMT2A; OMIM #609260), but our findings suggest that *MFN2* mutations may also underlie some human cases of connatal INAD.

METHODS

Animals

Dogs used in this study were members of a breeding colony maintained initially at University of Pennsylvania and later at Michigan State University. All dogs were handled according to the principles outlined in the NIH Guide for the Care and Use of Laboratory Animals. The respective Institutional Animal Care and Use Committees approved all protocols for routine care, breeding and whelping, and euthanasia. Dogs were of a large outbred family in which FNAD segregated as a fully penetrant, simple autosomal recessive trait (Fig. 1a). We determined disease status at birth by observation of a characteristic constellation of gross abnormalities, including joint contractures, scoliosis, cerebellar hypoplasia, and respiratory failure. Blood or tissue samples were stored frozen at −80° C for DNA isolation.

Markers and genotyping

We isolated DNA and performed an initial genome-wide scan using 152 simple sequence repeat (SSR) markers and DNA samples from a subpedigree of 172 dogs using previously described methods [12]. The Mammalian Genotyping Service of the National Heart, Lung, and Blood Institute, Marshfield Clinic Research Foundation, (Marshfield, WI) conducted a second genome-wide scan using a partially overlapping set of 249 SSR markers, 181 DNA samples, and similar methods. Both scans together assessed 329 previously published markers and 4 new SSR markers. Table 1 shows IDs, coordinates, and amplifying primers of 4 new SSR markers first developed for this study. We fine-mapped the linked region using samples from a subpedigree to assess segregation of single nucleotide polymorphism (SNP) alleles. We determined novel SNP sites (Table 1) by sequencing PCR products amplified from genomic DNA of obligate carrier dogs, as described [12].

Segregation of SNP alleles was determined by sequencing or by inference from appropriate restriction enzyme digests of PCR products.

Genetic linkage analysis

We computed LOD scores with Superlink [13]. We modeled the disease as a fully penetrant autosomal recessive trait, disease allele frequency as 0.01, and allele frequencies for each marker as equal. For multipoint analysis, we estimated inter-marker recombination fractions from the FNAD pedigree and its genotypes. We show results obtained in a single 170-dog subpedigree, although other subpedigrees were used for analysis in earlier stages of the project. We used e-PCR [14] to identify marker positions, and TBLASTN [15, 16] and MegaBLAST [17] to find matches for human exons on the dog sequence assemblies CanFam1 [18] and CanFam2 [19].

Gene sequencing

We sequenced the coding regions of genes within the critical interval, either by sequencing each exon with flanking intron-exon boundaries amplified from genomic DNA or by sequencing overlapping segments of cDNA produced by reverse transcription (RT) coupled PCR of RNA isolated from frozen brainstem, as described [20]. Contigs were assembled and aligned with orthologous sequences of other species using the Lasergene® software package (DNAstar®, Inc., Madison, WI). cDNA sequences were submitted to GenBank®.

MFN2 mutation detection and expression analysis

We detected mutant and normal *MFN2* alleles in genomic DNA by *Mnl I* digestion of a 264 bp PCR product amplified using primers 5′-GACGTGGCTTCTCCTCATCTCC-3′ and 5′-CACTGCTTGCCTGGTCATTGTAG-3′. We assessed expression of *MFN2* mRNA by RT-PCR of RNA isolated from brainstem of $MFN2^{+/+}$, $MFN2^{+/FNAD}$, and $MFN^{FNAD/FNAD}$ littermates. RT reactions were primed with oligo-dT, and PCR primers were 5′-CAGCAGGACATGATAGATGGTTTGAA-3′ (c.1480–1505, overlapping the exon 12/13 boundary) and 5′-ACAACGAGAATGCCCATGGAGGT-3′ (c.1840–1862, in exon 14). We discriminated allele-specific mRNA expression by *Mnl I* digestion of the 383 bp RT-PCR products.

For western blots, fresh tissue was homogenized and separated into fractions of total homogenate, mitochondria, microsomes (disrupted endoplasmic reticulum vesicles), and cytoplasm by differential centrifugation, as previously described [21]. We determined total protein concentrations by the Bradford method [22] and assessed MFN2 and control protein expression in each fraction on western blots, prepared as previously described [23]. Rabbit polyclonal antibody to VDAC/porin (ab15895; 40 ng/mL working concentration), chicken polyclonal antibody to calreticulin (ab14234; 330 ng/mL), affinity-purified chicken polyclonal antibody to mouse mitofusin 1 (MFN1) (ab60939; 1.5 μg/mL), and mouse monoclonal antibodies to MFN2 (ab56889; 3 μg/mL) and to α-tubulin (ab28037; 500 ng/mL) were obtained from Abcam, Inc. (Cambridge, MA). The anti-MFN2 antibody was raised against a 90-residue recombinant peptide representing human MFN2 residues 661–757, differing from the dog sequence at only 2 positions, and detected an 86 kDa protein on western blots of HeLa cell lysate (manufacturer's fact sheet). The anti-MFN1 antibody was raised against a fusion protein containing residues 348–579 of mouse MFN1, a region 94% identical to dog MFN1 but only 52% identical to dog MFN2, and detected an 84 kDa protein on western blots of mouse embryonic fibroblast lysates. Specificity was confirmed using lysates of cells derived from MFN1-null, MFN2-null, and double null embryos (manufacturer's fact sheet). Horse radish peroxidase (HRP) conjugates of rabbit anti-chicken IgY (A9792; diluted 1:180,000), goat anti-rabbit IgG (A9169; diluted 1:80,000), and rabbit anti-mouse IgG (A9044; diluted 1:80,000) were from Sigma Aldrich (St. Louis, MO). We

detected immunocrossreactive proteins by chemiluminescent reaction (Western Lightning Detection Kit, Perkin-Elmer, Waltham, MA) on blots exposed to film.

We performed immunohistochemistry on formalin fixed and paraffin embedded tissue samples using the monoclonal anti-MFN2 (1:250 dilution) and polyclonal chicken anti-MFN1 antibodies (1:100 dilution) described above. Secondary antibodies were biotinylated horse anti-mouse IgG (Vector Laboratories, Inc., Burlingame, CA) and biotinylated donkey anti-chicken IgY (Jackson ImmunoResearch Laboratories, Inc., West Grove, PA), respectively. We detected antibody binding by sequential incubation of slides in avidin-peroxidase (R.T.U. peroxidase reagent) and NovaRED™ peroxidase substrate as chromogen, both from Vector Laboratories, Inc. Images were acquired on a Nikon Eclipse 90i® microscope with a digital imaging camera. There was no image processing other than global adjustment of brightness and/or contrast.

RESULTS

Genome-wide linkage studies using a total of 329 previously published microsatellite markers failed to yield a statistically significant LOD score for FNAD so we further examined chromosome telomeres. The most telomeric marker used on CFA2 was FH2062, located 8.8 Mb from the telomere. Its peak LOD score was 1.64 at a recombination fraction (θ) of 0.29 (Table 2), which was the highest LOD score achieved by the most extreme marker on any chromosome. We identified four more SSRs, designated C02p027, 0258, C02p024, C02p014, between FH2062 and the telomere, and each of these achieved a LOD score of >15. In multipoint analysis using the four new markers, the peak LOD score for placing the gene between C02p027 and C02p024 was 36.1 and was >5 LOD units better than any other placement. FH2062 and C02p027 are separated by only 5.4 Mb, but the recombination fraction between them in this pedigree was 0.20. The high rate of recombination often encountered near chromosome ends [24] explained our failure to identify the disease locus using the previously established dog linkage markers.

The identified segment of CFA2 corresponds to the telomeric end of the short arm of human chromosome 1 (HSA1p). Comparative sequence analysis using BLAT [25] verified the locations of canine orthologs of HSA1p genes on CanFam1 [18] and CanFam2 [19]. Orthologous genes occurred in consistent, but opposite order in the two species, except that the dog ortholog of *VPS13D* appeared partially duplicated on CFA9, and there is an ~98 kb gap (CFA2:86.92–87.02 Mb) in the CanFam2 assembly.

Known and novel SNPs in or near several positional candidate genes on CFA2 were genotyped in dogs that had imperfect segregation of alleles in the nearest microsatellites and in some of their first-degree relatives. Three informative SNPs (C02ps502, rs22798447, and rs22793152) and SSRs flanking the interval were used as markers in single and multipoint linkage analysis (Tables 2 and 3). In multipoint analysis using various combinations of two or three markers at a time and a LOD score difference threshold of 3.0, we assessed the likelihood that the disease locus was to one side or the other or between marker pairs (Table 3). It followed statistically that the FNAD gene was between the markers in *TNFRSF1B* and *KIAA2013*. Furthermore, haplotype analysis (Fig. 1b) identified interval-defining recombination events at C02ps503 and rs22798447, telomeric of *TNFRSF1B* and in *KIAA2013* intron 2, respectively, thereby narrowing the critical interval to ~ 200 kb and abrogating concern about a potential *VPS13D* duplication.

There are 4 complete gene sequences in the human and canine genomes between *TNFRSF1B* and *KIAA2013* (Fig. 1c). We sequenced full coding regions of *PLOD1*, *MIIP*, and *MFN2* (GenBank® accession nos. GQ892932–GQ892934, respectively) in cDNA

amplified from brainstem RNA of an affected pup and a heterozygous littermate. The coding regions of *TNFRSF8* and *KIAA2013* that were within the critical interval were sequenced by amplifying exons and flanking splice sites from genomic DNA. Single nucleotide sequence variations were observed in each gene except *KIAA2013*. In *MIIP*, c.G241A and c.G290A predicted amino acid changes p.G81S and p.R97H, respectively, and c.T672C predicted no change. In *PLOD1*, c.T917G and c.G929A predicted amino acid substitutions p.L306R and p.R310H, respectively, and c.C865T predicted no change. In *TNFRSF8*, the only variation found was the protein synonymous SNP rs22781397.

In *MFN2*, there were 5 translationally silent sequence variations (c.T274C, c.A336G, c.T720C, c.G1053A, and c.C1252A) and 3 differences from the published dog genome sequence in the 3′ untranslated region (c.A2331T, c.T2368C, and c.A2465G). Most notably, there was a homozygous 3 bp deletion (c.1617_1619delGGA) in the affected pup cDNA sequence (confirmed in genomic DNA) that predicted an in-frame loss of a single glutamate residue (p.E539del). The deleted nucleotides are among a 2-unit trinucleotide repeat (GGAGGA) sequence as well as a longer symmetric element (CAGGAGGAC), which suggests that the mechanism of deletion may be DNA replication slippage [26, 27]. E539 is situated in a region of high conservation (the R5 region of conservation in Fig. 1 of [28]) among vertebrate and invertebrate MFN2 sequences, as well as those of the paralogue MFN1 (Fig. 1c). The deletion is between and somewhat removed from the more N-terminal heptad repeat (HR; aa 408–433) and the transmembrane (TM; aa 614–646) domains (Fig. 1d). The 3 bp deletion also obliterated an *Mnl I* restriction endonuclease recognition site that was used to genotype 172 dogs of the FNAD pedigree (Fig. 1e, lanes 1–3). All affected dogs were homozygous for loss of the cut site, and all obligate FNAD carriers were heterozygous. As a linkage marker, the *MFN2* mutation obtained a LOD score of 39.9 at $\theta = 0.0$ (Table 2).

We considered the predicted amino acid substitutions in *PLOD1* and *MIIP* as unlikely to be pathogenic because none of them was a highly conserved residue among mammals. Therefore, we investigated the effect of the *MFN2* deletion mutation on gene expression. To avoid confounding effects of brainstem pathology present in affected pups, allele-specific mRNA expression was assessed in histologically normal, heterozygote tissue as well as in homozygous-normal and affected tissue. As shown in lanes 4–6 of Fig. 1e, comparable amounts of *MFN2* RT-PCR product were amplified from brainstem RNA of normal, carrier, and affected pups, and fragments produced by *Mnl I* digestion of the amplification products correlated with the animals' genotypes, thus indicating the *MFN2* mutation had little effect on steady-state *MFN2* mRNA levels.

MFN2 protein expression was assessed by western blot in subcellular fractions of cerebrum, brainstem, kidney, and fibroblasts, representing CNS tissue that demonstrated no lesions or abundant neuroaxonal dystrophy, non-CNS tissue, and cultured primary cells, respectively. MFN2 was undetectable in any affected pup brainstem fraction, whereas organelle-specific loading controls were comparable in normal and affected littermate tissue (Fig. 1f). The mitochondrial and endoplasmic reticulum loading controls were enriched in their respective fractions. Increased protein loading and longer film exposure did not reveal MFN2 in any affected pup brainstem fraction (not shown). We found none of the four proteins examined in the cytosolic (post-microsomal) fractions, indicating that all are normally membrane associated. We did not readily detect MFN2 on western blots of affected pup cerebrum, kidney or cultured primary fibroblasts (Fig. 1g), indicating that the loss of MFN2 in brainstem was not due to the extensive neuropathology in that tissue. By over exposure of blots loaded with 3 fold more protein/lane (not shown), we observed faint, normally migrating bands of MFN2 immunoreactivity in affected pup kidney total homogenate and microsomal fractions, but not in the mitochondrial or cytosolic fractions, nor in the other tissues. Thereby, we estimated steady-state expression of MFN2 in affected pup kidney

fractions at levels 30–60 fold less than in the same fractions of normal littermate tissue. These results demonstrate that failure to detect the affected dog MFN2 in mitochondrial or microsomal fractions was likely due to protein instability rather than mistargeting.

Immunohistochemistry of normal pup brainstem sections demonstrated robust granular cytoplasmic staining of MFN2 in cerebellar Purkinje cells (Fig. 2b), deep cerebellar nuclei, and most large neurons in identified nuclei (Fig. 2f) or scattered in the myelencephalic tegmentum. There were many granules of staining throughout the neuropil, either isolated or in recognizable strands, that were most likely within neurites and/or glial cell processes. In contrast, MFN1 staining in normal pups, while robust in a few isolated cells throughout the brainstem (Fig. 2a and 2e), was minimal or absent from most Purkinje cells, those of the deep nuclei, the caudal olives, the nucleus of the 7th cranial nerve, and the tegmental giant cells. Little or no MFN1 staining was observed in the neuropil. There was no MFN2 staining in FNAD pup Purkinje cells, deep nuclei, or other parts of the brainstem (Fig. 2d and 2h). Distribution of MFN1 staining in the affected pups was similar to that in normal pup brainstem (Fig. 2c and 2g). Sporadic cells showed robust staining while others in the same nuclei or layers showed much fainter staining. There was never staining of either MFN1 or MFN2 in the dystrophic axons or spheroids (Fig. 2g and 2h).

DISCUSSION

Using a genetic linkage-based approach and gene expression analysis, we demonstrated that a novel homozygous mutation of the *MFN2* gene causes lethal, autosomal recessive FNAD in dogs [10]. Familial NAD has been described in dogs previously [29–35], but none have been of obviously fetal-onset, nor has a canine NAD-causing mutation been determined before. An in-frame, 3-nucleotide deletion in *MFN2* predicts loss of a single highly conserved residue (E539). The genetic lesion reduced immunodetectable MFN2 protein to nil in CNS and very low in other tissues, indicating that the disease pathology is due to loss of one or more MFN2-mediated functions. Loss of E539 most likely destabilizes the protein through misfolding or loss of a crucial protein-protein interaction. Altered organellar targeting remains a possibility, but there was no evidence in this study to support such a mechanism.

Canine FNAD is characterized by segmental swellings of axons with intact myelin sheaths throughout the brainstem extrapyramidal system, spinal cord and peripheral nerves. Axonal swellings of affected pups were filled with membrane bound fragments of variably degenerated mitochondria and other tubulomembranous material embedded in disorganized whorls of neurofilaments [10]. This pathology is similar to that in human patients exhibiting INAD caused by *PLA2G6* mutations or neurodegeneration with brain iron accumulation (NBIA1; a.k.a. PKAN; OMIM # 234200) caused by mutations of mitochondrial pantothenate kinase (*PANK2*). The same lesions were observed in mouse *Pla2g6* knockout models [36–38] but not in a *Pank2* knockout [39, 40], most likely because PANK2 only obtained mitochondrial targeting during primate evolution [41]. The pathophenotypic overlap of NBIA1 and INAD (a.k.a. NBIA2A) has caused some to hypothesize that *PLA2G6* and *PANK2* mutations each lead to lipid dyshomeostasis affecting mitochondrial function [6]. Finding that an *MFN2* mutation can cause similar neuronal lesions may emphasize the aspect of mitochondrial dysfunction in this hypothesis, though it remains hampered by incomplete understanding of the multiple functions of proteins encoded by these three disease-associated genes.

The canine FNAD phenotype is unique among species expressing known *MFN2* mutations. More than 70 distinct *MFN2* mutations in humans have been associated with Charcot-Marie-Tooth type 2A2 (CMT2A2; OMIM #609260) and hereditary motor and sensory neuropathy

with optic atrophy (HMSN VI or CMT6; OMIM #601152) according to the collections at the Inherited Peripheral Neuropathies Mutation Database (http://www.molgen.ua.ac.be/cmtmutations/Mutations/Default.cfm) and the Human Gene Mutation Database (http://www.hgmd.cf.ac.uk/ac/all.php), both accessed on March 22, 2011. Both disorders are axonal type peripheral neuropathies of variable age onset and predominantly autosomal dominant inheritance. NAD is not a pathologic feature described in either of these human disorders or in mouse models of *Mfn2* deficiency by gene knockout or mutant *Mfn2* transgene overexpression. Almost all *MFN2* mutations in humans are missense changes clustered in regions including and flanking the GTPase and heptad-repeat domains (Fig. 1d). No single-residue mutation until now has been described in the interval surrounding E539. Hence, the canine FNAD phenotype may be mutation-specific, rather than species-specific. Recently, a disease-associated SNP was identified in Tyrolean grey cattle that alters a putative exonic splice enhancer in *MFN2* exon 20, although there was no functional proof of disease causation [42]. The affected cattle exhibited neurodegeneration in peripheral nerve, spinal cord and brainstem, but NAD was not reported.

MFN1 and MFN2 are paralogous outer membrane-anchored proteins that mediate tethering in the initial step of mitochondrial fusion [43]. Pre-fusion tethering of mitochondria occurs via homotypic and heterotypic interactions of the 2 proteins. MFN1 and MFN2 have similar protein domain structures and overlapping but not identical tissue and subcellular expression profiles, protein-binding partners, and functions [44–51; reviewed in 51]. Importantly, while MFN1 and MFN2 can each at least partially complement the fusion function of the other when expressed in the same cells [52], there are at least two potentially important functional differences unrelated to mitochondrial fusion. In addition to mitochondria, MFN2 is also expressed in the ER membrane cytosolic leaflet mediating ER-mitochondrial contacts and is required for normal ER morphology and function [53], including supply of membrane lipids for autophagosomes [54]. MFN2 has also been identified in a complex that tethers mitochondria to microtubule-based molecular motors for axonal transport [55].

A remarkable aspect of the pattern of neuronal pathology in canine FNAD, particularly in the brain stem, is its specificity [10]. Specific cell types and nuclei are extensively abnormal while adjacent cells or nuclei are not. For instance, Purkinje cells, neurons of the deep cerebellar nuclei, the red nuclei, the caudal olivary nuclei, the myelencephalic tegmental giant cells, and the nuclei of the 5th and 7th cranial nerves show severe neuronal degeneration and/or axonal swelling, while the 3rd, 4th, 6th, and 12th cranial nerve nuclei and the rostral olivary nuclei are essentially normal. In this study the neurons and nuclei of FNAD pup brainstem showing the least MFN1 staining were those exhibiting the most extensive NAD and neuronal degeneration. This is compatible with the idea that complementation by MFN1 maintains sufficient neuronal homeostasis when a function(s) is lost due to MFN2 deficiency, a hypothesis advanced to explain observations of seemingly normal post-implantation development but post-natal cerebellar Purkinje cell degeneration in conditional *Mfn2*$^{-/-}$ knockout mice [50]. Those authors further demonstrated that mouse Purkinje cells express abundant *Mfn2*, but little or no *Mfn1* mRNA, similar to our findings by immunohistochemistry in newborn dogs. While this provides a plausible basis for cell-type specific degeneration of Purkinje cells and other brainstem neurons, it may be premature to conclude that mitochondrial fusion is the only neuron-preserving function provided by MFN1 to complement MFN2 deficiency. It is evident, however, that sufficient mitofusin function, considered broadly, is maintained in crucial tissues of homozygous mutant dog embryos to support implantation and near-normal development until late in gestation. The survival of the FNAD fetus could be due to either MFN1 complementation or to low-level and perhaps tissue-specific expression of the mutant MFN2, especially earlier than the last half of the third trimester which we have not yet examined.

Dominant inheritance of the majority of human CMT2A2 mutations in *MFN2* suggests they cause disease by gain-of-function, dominant-negative effects, or haploinsufficiency. In contrast, recessive inheritance of the dog disorder indicates that theirs is a loss-of-function allele. Determining the mechanism by which the E539del *MFN2* mutation causes dystrophy and degeneration in dogs may reveal a new aspect of neuroaxonal development and homeostasis.

Acknowledgments

FUNDING: This work was supported by the National Institutes of Health [NS41989, RR02512 and contract HV48141]; the Purebred Dog Endowment Fund, College of Veterinary Medicine, Michigan State University; and in part by the Intramural Research Program of the NIH, NLM. Author RAA was supported by a Department of Pathology Scholarship for Basic Medical Sciences (KU-984) from the Kuwait University Faculty of Medicine.

References

1. Khateeb S, Flusser H, Ofir R, Shelef I, Narkis G, Vardi G, Shorer Z, Levy R, Galil A, Elbedour K, Birk OS. *PLA2G6* mutation underlies infantile neuroaxonal dystrophy. Am J Hum Genet. 2006; 79:942–948. [PubMed: 17033970]
2. Morgan NV, Westaway SK, Morton JEV, et al. *PLA2G6*, encoding a phospholipase A2, is mutated in neurodegenerative disorders with high brain iron. Nat Genet. 2006; 38:752–754. [PubMed: 16783378]
3. Aicardi J, Castelein P. Infantile neuroaxonal dystrophy. Brain. 1979; 102:727–748. [PubMed: 509195]
4. Kurian MA, Morgan NV, MacPherson L, et al. Phenotypic spectrum of neurodegeneration associated with mutations in the *PLA2G6* gene (PLAN). Neurology. 2008; 70:1623–1629. [PubMed: 18443314]
5. Gregory A, Westaway SK, Holm IE, et al. Neurodegeneration associated with genetic defects in phospholipase A_2. Neurology. 2008; 71:1402–1409. [PubMed: 18799783]
6. Gregory A, Polster BJ, Hayflick SJ. Clinical and genetic delineation of neurodegeneration with brain iron accumulation. J Med Genet. 2009; 46:73–80. [PubMed: 18981035]
7. Jennekens FGI, Barth PG, Fleury P, Veldman H, Keuning JF, Westdorp J. Axonal dystrophy in a case of connatal thalamic and brain stem degeneration. Acta Neuropathol. 1984; 64:68–71. [PubMed: 6089496]
8. Chow G, Padfield CJH. A case of infantile neuroaxonal dystrophy-connatal Seitelberger disease. J Child Neurol. 2008; 23:418–420. [PubMed: 18287574]
9. Rakheja D, Uddin N, Mitui M, Cope-Yokoyama S, Hogan RN, Burns DK. Fetal akinesia deformation sequence and neuroaxonal dystrophy without *PLA2G6* mutation. Pediatr Dev Pathol. 2010; 13:492–496. [PubMed: 20235854]
10. Fyfe JC, Al-Tamimi RA, Castellani RJ, Rosenstein D, Goldowitz D, Henthorn PS. Inherited neuroaxonal dystrophy in dogs causing lethal, fetal-onset motor system dysfunction and cerebellar hypoplasia. J Comp Neurol. 2010; 518:3771–3784. [PubMed: 20653033]
12. He Q, Fyfe JC, Schäffer AA, Kilkenney A, Werner P, Kirkness EF, Henthorn PS. Canine Imerslund-Gräsbeck syndrome maps to a region orthologous to HSA14q. Mamm Genome. 2003; 14:758–764. [PubMed: 14722725]
13. Fishelson M, Geiger D. Exact genetic linkage computations for general pedigrees. Bioinformatics. 2002; 18(Suppl 1):S189–198. [PubMed: 12169547]
14. Schuler GD. Sequence mapping by electronic PCR. Genome Res. 1997; 7:541–550. [PubMed: 9149949]
15. Altschul SF, Madden TL, Schäffer AA, Zhang J, Zhang Z, Miller W, Lipman DJ. Gapped BLAST and PSI-BLAST—a new generation of protein database search programs. Nucleic Acids Res. 1997; 25:3389–3402. [PubMed: 9254694]

16. Gertz EM, Yu Y-K, Agarwala R, Schäffer AA, Altschul SF. Composition-based statistics and translated nucleotide searches: improving the TBLASTN module of BLAST. BMC Biol. 2006; 4:41. [PubMed: 17156431]
17. Zhang Z, Schwartz S, Wagner L, Miller W. A greedy algorithm for aligning DNA sequences. J Comput Biol. 2000; 7:203–214. [PubMed: 10890397]
18. Kirkness EF, Bafna V, Halpern AL, Levy S, Remington K, Rusch DB, Delcher AL, Pop M, Wang W, Fraser CM, Venter JC. The dog genome: Survey sequencing and comparative analysis. Science. 2003; 301:1898–903. [PubMed: 14512627]
19. Lindblad-Toh K, Wade CM, Mikkelsen TS, et al. Genome sequence, comparative analysis, and haplotype structure of the domestic dog. Nature. 2005; 438:803–819. [PubMed: 16341006]
20. Gregory BL, Shelton GD, Bali DS, Chen Y-T, Fyfe JC. Glycogen storage disease type IIIa in curly-coated retrievers. J Vet Intern Med. 2007; 21:40–46. [PubMed: 17338148]
21. Sujkovic E, Mileusnic R, Fry JP. Metabolism of neuroactive steroids in day old chick brain. J Neurochem. 2009; 109:348–359. [PubMed: 19200338]
22. Bradford MM. A rapid and sensitive method for the quantitation of microgram quantities of protein utilizing the principle of protein-dye binding. Anal Biochem. 1976; 72:248–254. [PubMed: 942051]
23. Xu D, Fyfe JC. Cubilin expression and posttranslational modification in the canine gastrointestinal tract. Am J Physiol Gastrointest Liver Physiol. 2000; 279:G748–756. [PubMed: 11005762]
24. Kong A, Gudbjartsson DF, Sainz J, et al. A high-resolution recombination map of the human genome. Nat Genet. 2002; 31:241–247. [PubMed: 12053178]
25. Kent WJ. BLAT - the BLAST-like alignment tool. Genome Res. 2002; 12:656–664. [PubMed: 11932250]
26. Krawczak M, Cooper DN. Gene deletions causing human genetic disease: mechanisms of mutagenesis and the role of the local DNA sequence environment. Hum Genet. 1991; 86:425–441. [PubMed: 2016084]
27. Ball EV, Stenson PD, Abeysinghe SS, Krawczak M, Cooper DN, Chuzhanova NA. Microdeletions and microinsertions causing human genetic disease: Common mechanisms of mutagenesis and the role of local DNA sequence complexity. Hum Mutat. 2005; 26:205–213. [PubMed: 16086312]
28. Honda S, Aihara T, Hontani M, Okubo K, Hirose S. Mutational analysis of action of mitochondrial fusion factor mitofusin-2. J Cell Sci. 2005; 118:3153–3161. [PubMed: 15985463]
29. Cork LC, Troncoso JC, Price DL, Stanley EF, Griffin JW. Canine neuroaxonal dystrophy. J Neuropathol Exper Neurol. 1983; 42:286–296. [PubMed: 6842267]
30. Griffiths IR, Duncan ID. The central nervous system in canine giant axon neuropathy. Acta Neuropathol. 1979; 46:169–172. [PubMed: 223361]
31. Sacre BJ, Cummings JF, de Lahunta A. Neuroaxonal dystrophy in a Jack Russell terrier pup resembling human infantile neuroaxonal dystrophy. Cornell Vet. 1993; 83:133–142. [PubMed: 8467699]
32. Diaz JV, Duque C, Geisel R. Neuroaxonal dystrophy in dogs: Case report in 2 litters of papillon puppies. J Vet Intern Med. 2007; 21:531–534. [PubMed: 17552463]
33. Jäderlund KH, Örvind E, Johnsson E, Matiasek K, Hahn CN, Malm S, Hedhammar Å. A neurologic syndrome in golden retrievers presenting as a sensory ataxic neuropathy. J Vet Intern Med. 2007; 21:1307–1315. [PubMed: 18196741]
34. Nibe K, Kita C, Morozumi M, Awamura Y, Tamura S, Okuno S, Kobayashi T, Uchida K. Clinicopathological feature of canine neuroaxonal dystrophy and cerebellar cortical abiotrophy in papillon and papillon-related dogs. J Vet Med Sci. 2007; 69:1047–1052. [PubMed: 17984592]
35. Nibe K, Nakayama H, Uchida K. Immunohistochemical features of dystrophic axons in papillon dogs with neuroaxonal dystrophy. Vet Pathol. 2009; 46:474–483. [PubMed: 19176506]
36. Shinzawa K, Sumi H, Ikawa M, Matsuoka Y, Okabe M, Sakoda S, Tsujimoto Y. Neuroaxonal dystrophy caused by group VIA phospholipase A_2 deficiency in mice: a model of human neurodegenerative disease. J Neurosci. 2008; 28:2212–2220. [PubMed: 18305254]
37. Malik I, Turk J, Mancuso DJ, Montier L, Wohltmann M, Wozniak DF, Schmidt RE, Gross RW, Kotzbauer PT. Disrupted membrane homeostatis and accumulation of ubiquinated proteins in a

mouse model of infantile neuroaxonal dystrophy caused by *PLA2G6* mutations. Am J Pathol. 2008; 172:406–416. [PubMed: 18202189]

38. Wada H, Yasuda T, Miura I, Watabe K, Sawa C, Kamijuku H, Kojo S, Taniguchi M, Nishino I, Wakana S, Yoshida H, Seino K. Establishment of an improved mouse model for infantile neuroaxonal dystrophy that shows early disease onset and bears a point mutation in *Pla2g6*. Am J Pathol. 2009; 175:2257–2263. [PubMed: 19893029]
39. Kuo Y-M, Duncan JL, Westaway SK, Yang H, Nune G, Xu EY, Hayflick SJ, Gitschier J. Deficiency of pantothenate kinase 2 (*Pank2*) in mice leads to retinal degeneration and azoospermia. Hum Mol Genet. 2005; 14:49–57. [PubMed: 15525657]
40. Kuo YM, Hayflick SJ, Gitschier J. Deprivation of pantothenic acid elicits a movement disorder and azoospermia in a mouse model of pantothenate kinase-associated neurodegeneration. J Inherit Metab Dis. 2007; 30:310–317. [PubMed: 17429753]
41. Leonardi R, Zhang Y-M, Lykidis A, Rock CO, Jackowski S. Localization and regulation of mouse pantothenate kinase 2. FEBS Lett. 2007; 581:4639–4644. [PubMed: 17825826]
42. Drögemüller C, Reichart U, Seuberlich T, et al. An unusual splice defect in the mitofusin 2 gene (*MFN2*) is associated with degenerative axonopathy in Tyrolean grey cattle. PloS One. 2011; 6:e18931. [PubMed: 21526202]
43. Meeusen SL, Nunnari J. How mitochondria fuse. Curr Opin Cell Biol. 2005; 17:389–394. [PubMed: 15975776]
44. Bach D, Pich S, Soriano FX, et al. Mitofusin-2 determines mitochondrial network architecture and mitochondrial metabolism. J Biol Chem. 2003; 278:17190–7. [PubMed: 12598526]
45. Santel A, Frank S, Gaume B, Herrier M, Youle RJ, Fuller MT. Mitofusin-1 protein is a generally expressed mediator of mitochondrial fusion in mammalian cells. J Cell Sci. 2003; 116:2763–2774. [PubMed: 12759376]
46. Ishihara N, Eura Y, Mihara K. Mitofusin 1 and 2 play distinct roles in mitochondrial fusion reactions via GTPase activity. J Cell Sci. 2004; 117:6535–6546. [PubMed: 15572413]
47. Nakamura N, Kimura Y, Tokuda M, Honda S, Hirose S. MARCH-V is a novel mitofusin 2- and Drp1-binding protein able to change mitochondrial morphology. EMBO Reports. 2006; 7:1019–1022. [PubMed: 16936636]
48. Hájek P, Chomyn A, Attardi G. Identification of a novel mitochondrial complex containing mitofusin 2 and stomatin-like protein 2. J Biol Chem. 2007; 282:5670–5681. [PubMed: 17121834]
49. Chen H, Detmer SA, Ewald AJ, Griffin EE, Fraser SE, Chan DC. Mitofusins Mfn1 and Mfn2 coordinately regulate mitochondrial fusion and are essential for embryonic development. J Cell Biol. 2003; 160:189–200. [PubMed: 12527753]
50. Chen H, McCaffery JM, Chan DC. Mitochondrial fusion protects against neurodegeneration in the cerebellum. Cell. 2007; 130:548–562. [PubMed: 17693261]
51. Liesa M, Palacín M, Zorzano A. Mitochondrial dynamics in mammalian health and disease. Physiol Rev. 2009; 89:799–845. [PubMed: 19584314]
52. Detmer SA, Chan DC. Complementation between mouse Mfn1 and Mfn2 protects mitochondrial fusion defects caused by CMT2A disease mutations. J Cell Biol. 2007; 176:405–414. [PubMed: 17296794]
53. de Brito OM, Scorrano L. Mitofusin-2 tethers endoplasmic reticulum to mitochondria. Nature. 2008; 456:605–610. [PubMed: 19052620]
54. Hailey DW, Rambold AS, Satpute-Krishnan P, Mitra K, Kim PK, Lippincott-Schwartz J. Mitochondria supply membranes for autophagosome biogenesis during starvation. Cell. 2011; 141:656–667. [PubMed: 20478256]
55. Misko A, Jiang S, Wegorzeska I, Milbrandt J, Baloh RH. Mitofusin 2 is necessary for transport of axonal mitochondria and interacts with the Miro/Milton complex. J Neurosci. 2010; 30:4232–4240. [PubMed: 20335458]
56. Wong AK, Neff MW. *DOGSET*: pre-designed primer sets for fine-scale mapping and DNA sequence interrogation in the dog. Anim Genet. 2009; 40:569–571. [PubMed: 19392818]
57. Rojo M, Legros F, Chateau D, Lombès A. Membrane topology and mitochondrial targeting of mitofusins, ubiquitous mammalian homologs of the transmembrane GTPase Fzo. J Cell Sci. 2002; 115:1663–1674. [PubMed: 11950885]

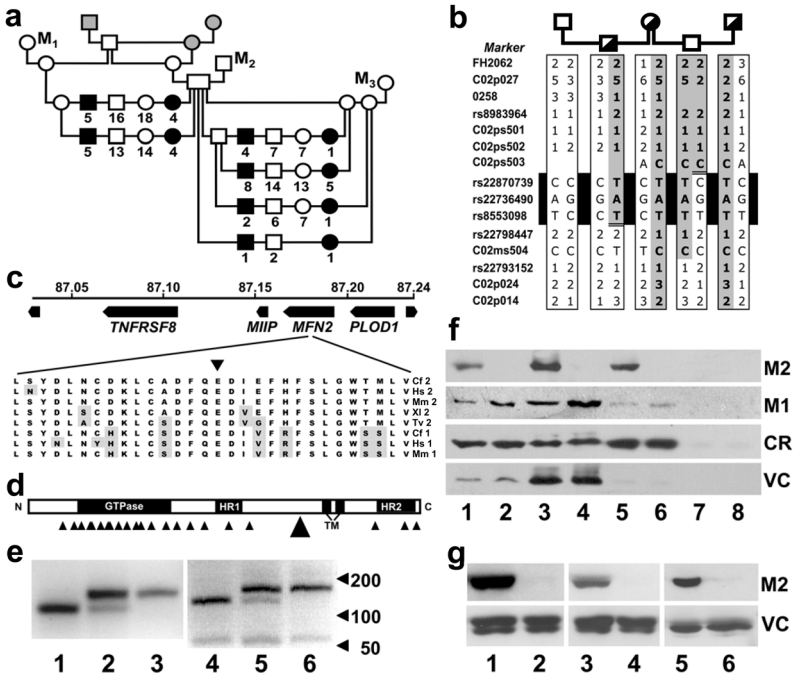

Fig. 1.

Genetic findings in canine FNAD. **a** Mapping pedigree. Squares indicate males, circles indicate females and filled symbols indicate FNAD affected offspring. Numbers below symbols indicate the total offspring of the indicated mating, sex, and phenotype. The 3 gray shaded symbols indicate dogs that were not genotyped in this investigation, and $M_{1–3}$ indicate 3 mongrel dogs used in outcross matings. **b** Haplotype analysis. Genotypes were determined at multiple SSR and SNP markers at the telomeric end of CFA2. Half-filled symbols indicate obligate carriers. Haplotypes were assembled by inference from parental genotypes, and the parental haplotype harboring the disease mutation (shaded) was determined by genotyping an affected pup (not shown). Recombinations of markers rs22870739 and rs8553098 defined a critical interval of ~200 kb. **c** Schematic of the *MFN2* mutation site. Four genes in the disease locus, their coordinates on CFA2, and direction of transcription are shown. A 3 bp deletion in exon 14 eliminates the highly conserved E539 residue (inverted triangle) from the *MFN2* translation product. Cf 2, Hs 2, Mm 2, Xl 2, and Tv 2 indicate MFN2 sequences of dog, human, mouse, clawed frog, and pufferfish, respectively. Cf 1, Hs 1, and Mm 1 indicate MFN1 sequences of the indicated species. Residues that differ from the dog MFN2 sequence are shaded. **d** Domain structure of MFN2. HR1 and HR2 are heptad repeat domains, and TM indicates a bipartite transmembrane domain that presents both the N- and C-terminal domains to the cytoplasmic face of the mitochondrial outer and ER membranes [57]. Small arrowheads indicate the distribution of reported human CMT2A2 mutations. The large arrowhead indicates the canine FNAD mutation. **e** Allele-specific mutation detection. The 3-bp deletion mutation in *MFN2* obliterates an *Mnl I* endonuclease recognition site. PCR products of genomic (lanes 1–3) and cDNA (lanes 4–6) of genetically normal (lanes 1 and 4), obligate carrier (lanes 2 and 5), and FNAD affected (lanes 3 and 6) dogs were digested with *Mnl I* and electrophoresed. **f** Western blots of brainstem fractions. Frozen brainstem of a normal (lanes 1, 3, 5, and 7) and an FNAD affected pup (lanes 2, 4, 6, and 8) was homogenized and separated by differential centrifugation into total homogenate (lanes 1 and 2), mitochondrial (lanes 3 and 4), microsomal (lanes 5 and 6), and cytosolic fractions (lanes 7 and 8). Thirty μg of total protein/fraction were separated by SDS-PAGE. The resulting blot was incubated

sequentially with anti-MFN2 (M2), anti-MFN1 (M1), and antibodies against voltage-dependent anion channel/porin (VC) and calreticulin (CR) used as mitochondrial and ER protein loading controls, respectively. **g** Western blots of cerebrum, kidney, and cultured fibroblasts. Thirty μg of total protein from cerebrum (lanes 1 and 2), kidney (lanes 3 and 4), and primary fibroblast lysates (lanes 5 and 6) of a normal (lanes 1, 3, and 5) and an FNAD affected pup (lanes 2, 4, and 6) were separated by SDS-PAGE. Resulting blots were incubated sequentially with anti-MFN2 (M2) and anti-VDAC (VC).

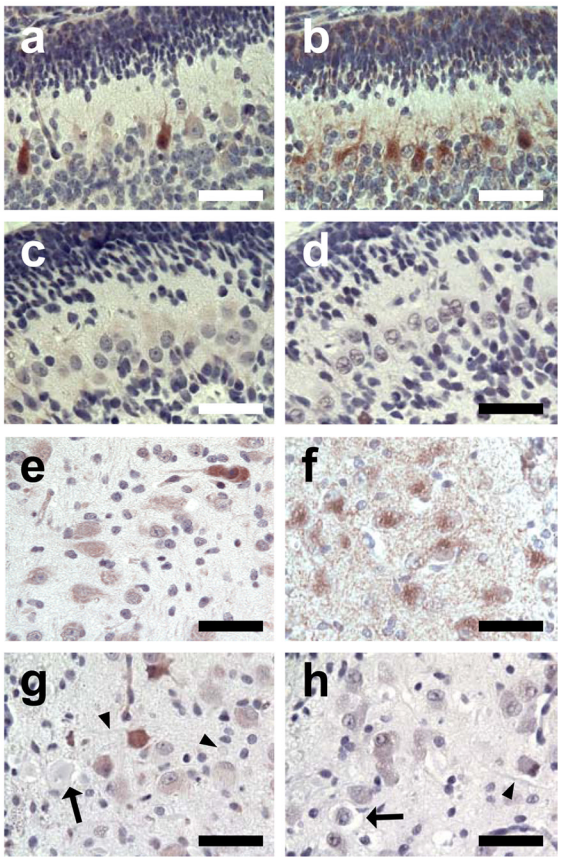

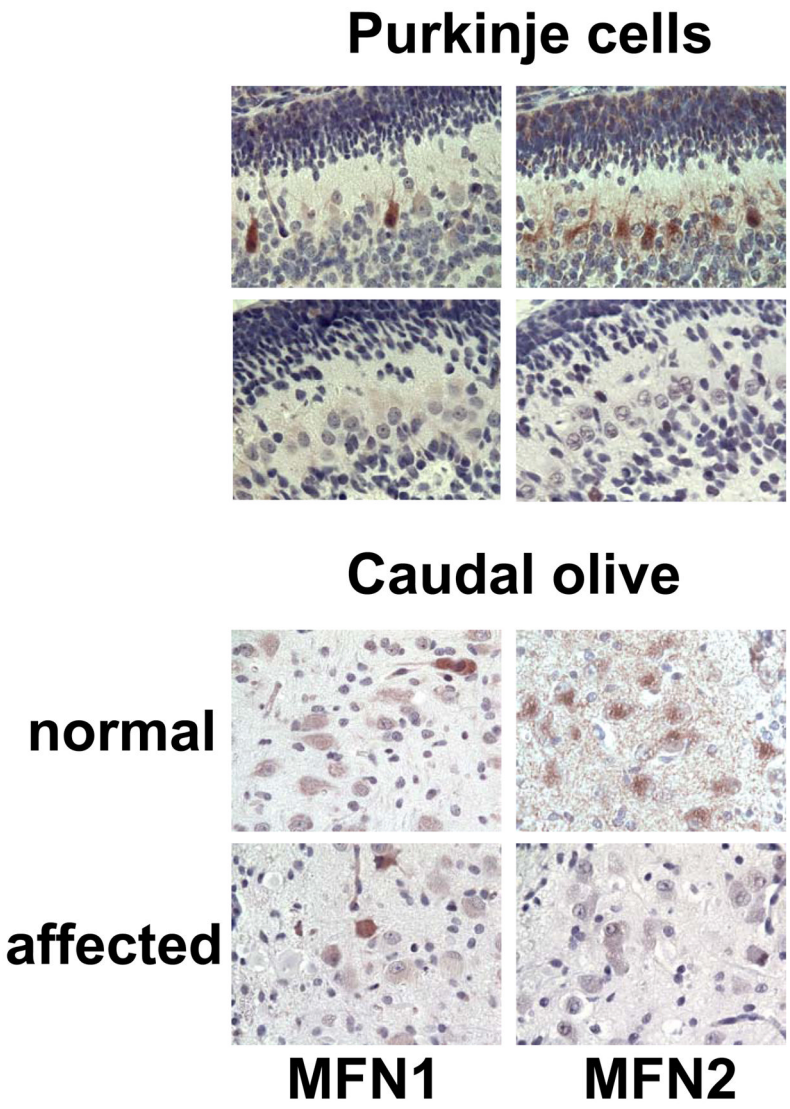

Fig. 2.

MFN2 and MFN1 expression in brainstem *in situ*. Formalin-fixed brainstem with cerebellum of a newborn normal pup (panels a, b, e, f) and an FNAD affected littermate (panels c, d, g, h) were processed for immunhistochemistry. Primary antibodies were anti-MFN1 (panels a, c, e, g) and anti-MFN2 (b, d, f, h). Panels a, b, c, and d show sections of cerebellum with exterior granular layer at the top. Panels e, f, g, and h show sections through the caudal olivary nucleus. In panels g and h, degenerating neurons (arrows), dystrophic axons, and spheroids (arrowheads) are lightly stained grey/blue with hematoxylin counterstain. Bars in each panel are 50 μm.

Table 1

Novel SSR and SNP markers used in this study.

Marker ID	CFA2 location*	Polymorphism Details §	Forward (F) and reverse (R) primers 5′ -> 3′
C02p027	85,058,262	SSR - $(CTTTT)_{15}$	F- CACCGCCCCGTTTGACAGG R- CTCGCCAGCCCCCACACCAC
0258†	86,044,331	SSR - $(AC)_{18}$	F- CTGAGAGGCACAGCCAACAC R- GCTCCTTCTTCGACGTGCTT
C02p024	87,685,847	SSR - $(CA)_{20}$	F- CCTTGGGGCCACATGACTTCTACC R- CTTTATTTCTGCGTGCCCTTGTGC
C02p014	88,241,450	SSR - $(CA)_{22}$	F- TCCCTGAATCCTGAGCAAAAT R- GCGGCCAGGATGTGTCAAAATA
C02ps501	86,795,606	SNP - A/G, in VPS13D 3′ UTR, *Hha I* digest	F- CACCCGCCCACGCTCTACACTCTG R- ACCCCTCACCCCTCACCCCTTACG
C02ps502	87,029,973	SNP - C/T, in TNFSRF1B intron	F- GGTGGGGCCGGCAGGTATC R- TAGCAGGGGCCGTGGTAAGAGTTT
C02ps503	87,039,470	SNP - A/C, centromeric of TNSRSF8	F- AACGGGGGACGGAGCCTTCTGC R- GCCGCCGCCTGTGATGTGGTCT
C02ms504	87,300,627	SNP - C/T, in CLCN6 intron, *Msp I* digest	F- AGGTGGCTGCAAGCAGGAGGAAC R- GTGGGTGTTGGGTGAAACGGTGA

* location of beginning of simple sequence repeat or SNP, based on CanFam2 dog genome assembly

§ SSR-simple sequence repeat; SNP-single nucleotide polymorphism; subscript indicates copy number in CanFam2 dog genome assembly

† see reference [56]

Table 2

Peak single marker scores for some informative markers at the telomeric end of CFA2. Recombination fractions are optimal to within 0.01. AHT111 and FH2062 are published microsatellites, and 0258 is a DOGSET marker [56]. C02p027, C02p024, and C02p014 are microsatellite markers developed for this study. SNPs rs22798447 and rs22793152 are in the dog genes *KIAA2013* and *FBXO2*, respectively. CO2ps502 is a new polymorphism in the dog gene *TNFRSF1B* identified in this study. *MFN*2del is the 3 bp deletion mutation in the gene *MFN2*, treated in this table as a genetic marker. The order of markers shown was proven with a combination of linkage and sequence analysis and corresponds to the CanFam2 dog genome sequence assembly.

Marker	Peak LOD score	Recombination fraction (θ)
AHT111	2.60	0.28
FH2062	1.64	0.29
C02p027	20.56	0.09
0258	15.24	0.03
CO2ps502	16.13	0.01
*MFN*2del	39.90	0.00
rs22798447	20.93	0.01
rs22793152	22.19	0.00
C02p024	27.77	0.01
C02p014	21.74	0.02

Table 3

Statistical inferences about the FNAD gene position using multipoint analysis. This table summarizes two-marker analyses in which we considered three possible locations for the gene: centromeric of marker A, between the markers, and telomeric of marker B. We compared the log likelihoods of the best positions for the gene in all three intervals and obtained a LOD score comparing the best position to either the second best or the worst. When the best position was at least 3.0 LOD units better than the second best, the other two locations were excluded. When the best position was at least 3.0 LOD units better than the worst, the worst location was excluded. The bottom row indicates a three-marker analysis. Combining the summarized analyses, we inferred that the FNAD gene was between markers C02ps502 and rs22798447.

Marker A	Marker B	Marker C	Inferred position of FNAD gene	Justifying LOD Score Difference
AHT111	neff0258		Telomeric of AHT111	10.49
AHT111	C02p027		Telomeric of C02p027	5.41
FH2062	C02p027		Telomeric of C02p027	5.08
FH2062	C02p024		Telomeric of FH2062	23.17
C02p027	C02ps502		Telomeric of C02p027	8.07
C02p027	rs22798447		Telomeric of C02p027	12.21
C02p027	C02p024		Between markers	3.07
C02p027	C02p014		Between markers	3.28
neff0258	rs22798447		Telomeric of 0258	3.39
C02ps502	C02p024		Telomeric of C02ps502	3.93
C02ps502	C02p014		Between markers	3.17
C02ps502	rs22798447	C02p014	Centromeric of rs22798447	3.19